Int. J. Heat Mass Transfer. Vol. 33, No. 6, pp. 1121–1134, 1990
Printed in Great Britain

0017-9310/90 $3.00+0.00

An analytical and experimental investigation of natural convection heat transfer in vertical channels with a single obstruction

S. A. M. SAID
Mechanical Engineering Department, King Fahd University of Petroleum and Minerals, Dhahran 31261, Saudi Arabia

and

R. J. KRANE
Mechanical and Aerospace Engineering, The University of Tennessee, Knoxville, TN 37996-2210, U.S.A.

(*Received* 28 *October* 1988 *and in final form* 11 *August* 1989)

Abstract—An experimental and numerical investigation was made of laminar natural convection flow of air in a vertical channel with a single obstruction. In the experimental study, optical techniques were used to obtain measurement of both quantitative data (heat fluxes and temperatures) and qualitative data (flow visualization). Only uniform wall temperature (UWT) boundary conditions were investigated experimentally. In the numerical study, a general purpose, finite element computer code called NACHOS was used. Thermal boundary conditions, uniform wall temperature (UWT), and uniform heat flux (UHF) were investigated numerically. The experimental and numerical results were in close agreement. The results indicate that for UWT boundary conditions the presence of an obstruction reduces the average Nusselt number by 5% at a Rayleigh number of 10^4 to about 40% at a Rayleigh number of 10. It is also noted that the location of the obstruction along the wall affects the rate of heat transfer. Moving the obstruction away from the entrance towards the exit reduces the average heat transfer rate for the channel. For UHF boundary conditions, the maximum temperature (which occurs at the intersection of the top edge of the obstruction and the wall) is only 4% higher than the maximum temperature for an unobstructed channel (which occurs at the exit of the channel).

1. INTRODUCTION

Steady-state natural convection flows in vertical channels are of interest in a number of engineering applications. One of these is the natural convection cooling of electronic cabinets containing circuit cards which are aligned to form vertical channels. The importance of heat transfer considerations in the design of electronic equipment has been reviewed by Aung and Chimah [1], Jaluria [2], and Kraus and Bar-Cohen [3]. Many diverse flow configurations are of interest in electronic cooling applications. The most important of these configurations is the vertical channel. Laminar, natural convection heat transfer in vertical channels has been investigated theoretically (on the basis of boundary layer equations), as well as experimentally. Representative contributions to the analytical literature on the subject have been made by several investigators. Engel and Mueller [4] analyzed the development of natural convection in channels of finite length for a wide range of Prandtl and Rayleigh numbers for both constant wall temperature and constant wall heat-flux boundary conditions. Bodoia and Osterle [5] investigated the development of free convection in an isothermal vertical channel by using the finite-difference method to numerically integrate the boundary layer equations. Aung *et al.* [6] investigated numerically and experimentally the development of free convection heat transfer in vertical channels with asymmetric heating. They considered both thermal boundary conditions of uniform wall heat fluxes and uniform wall temperature. Miyatake *et al.* [7] analyzed numerically the natural convection heat transfer between two vertical parallel plates where uniform heat flux is applied to one plate while the other is thermally insulated. In another study, Miyatake and Fujii [8] analyzed the same problem with one plate isothermally heated and the other thermally insulated. Aung *et al.* [9] studied numerically and experimentally natural convection cooling of arrays of vertically oriented circuit cards, aligned to form vertical channels or ducts. Coyne [10] investigated the same problem analytically. This analysis involves the calculation of steady-state, laminar, two-dimensional parabolic flow in vertical channels. Kettleborough [11] studied numerically the transient laminar free convection in a heated vertical channel. Nakamura *et al.* [12] performed a numerical analysis of the problem studied by Kettleborough, without using the boundary-layer approximation. Burch *et al.* [13] used a finite-difference procedure to investigate the problem of laminar natural convection between finitely conducting ver-

NOMENCLATURE

AR	aspect ratio of the channel, b/L
b	channel width
C_p	specific heat of fluid
g	magnitude of the acceleration due to gravity
Gr	Grashof number, $gb(T_w - T_\infty)b^3/v^2$
Gr^*	modified Grashof number, $gbq_w b^4/v^2 K$
K	fluid thermal conductivity
L	channel height
$\bar{L}_i$	obstruction height from channel entrance, see Fig. 1
$\bar{P}$	motion pressure
P	dimensionless pressure, $(P - P_\infty)/g\beta\rho_\infty(\Delta T)L$ for UWT
P^*	modified dimensionless pressure, $(P - P_\infty)K/gb\rho_\infty q_w bL$ for UHF
P_∞	hydrostatic fluid pressure
Pr	Prandtl number, v/a
q_w	wall heat flux
$\bar{r}$	obstruction radius, see Fig. 1
Ra	Rayleigh number, $Pr\ Gr$
Ra^*	modified Rayleigh number, $Pr\ Gr^*$
Ra'	Rayleigh number, $Ra\ AR$
$\bar{T}$	fluid temperature
ΔT	$T_w - T_\infty$
$\bar{u}$	x-component of velocity
u	dimensionless x-component of velocity, $\bar{u}b^2/\alpha L$
$\bar{v}$	y-component of velocity
v	dimensionless y-component of velocity, $\bar{v}b^2/\alpha$
$\bar{x}, \bar{y}$	spatial coordinates, see Fig. 4.

Greek symbols

α	thermal diffusivity
β	thermal expansion coefficient of fluid
θ	dimensionless temperature, $(T - T_\infty)/(T_w - T_\infty)$ for UWT
$\bar{\theta}$	dimensionless temperature, $(T - T_\infty)/(q_w b/k)$ for UHF
θ_{max}	dimensionless maximum temperature, $(T_{max} - T_\infty)/(q_w b/k)$ for UHF
μ	dynamic viscosity of fluid
v	kinetic viscosity of fluid
ρ	density of fluid.

Subscripts

i	refers to one of the vertical walls of the obstructed channel
max	maximum value
w	wall value
$\bar{x}$	value at distance x from channel entrance
∞	indicating the conditions at infinity.

tical plates. Carpenter *et al.* [14] investigated numerically the interaction of radiation with developing free convective heat transfer in vertical parallel plate channels with asymmetric heating. Aihara [15] studied the effect of inlet boundary conditions on the numerical solutions of free convection flow in vertical channels. The three-dimensional buoyancy-induced flow in a duct has been analyzed by Karki and Patankar [16] and Ramakrishna *et al.* [17]. Similar analysis for vertical circular tubes has been carried out by Davis and Perona [18], Kageyama and Izumi [19], and Dyer [20].

The original experimental study of natural convection between parallel plates is that of Elenbass [21]. His results are often compared with analytical results for parallel plate channels. Natural convection heat transfer measurements for vertical channels with isothermal walls of different temperature are presented in the work of Sernas *et al.* [22]. A recent experimental study by Sparrow and Bahrami [23] encompasses three types of hydrodynamic boundary conditions along the lateral edges of the channel. Akbari and Borges [24] solved numerically the two-dimensional, free convective, laminar flow in the Trombe wall channel, while Tichy [25] solved the same problem using an Oseen-type approximation. Levy *et al.* [26] address the problem of optimum plate spacings for laminar natural convection flow between two plates. Churchill [27], using the theoretical and experimental results obtained by a number of authors for the mean rate of heat transfer in laminar buoyancy driven flow through vertical channels, developed a general correlation equation for these results. Sparrow and Prakash [28] and Prakash and Sparrow [29] dealt with natural convection in vertical arrays of interrupted parallel plates. Aung *et al.* [9] attempted to derive a general expression to account for the effect of flow restriction, while still considering the governing equation to be parabolic. Flow restrictions encountered in Aung's study are in the form of staggered cards and baffles.

It can thus be concluded that unobstructed natural convection channel flows have been extensively investigated and that many aspects of these flows are now well understood.

When obstructions (protrusion from a channel wall) are located inside the channel, as encountered in many practical applications, the problem becomes elliptic. Very little is known of the natural convection phenomena in such complex flows [30]. Hence, the present study will be concerned with a combined experimental and numerical investigation of the laminar natural convection flow of air in a vertical channel with a single obstruction.

2. STATEMENT OF THE PROBLEM

The present study considers the two-dimensional, steady-state, laminar natural convection flow of a Newtonian fluid that occurs in the obstructed vertical channel shown in Fig. 1. A detailed statement and solution procedures of the problem are given in ref. [31]. The flows are assumed to be such that they can be adequately modeled by the Boussinesq approximation [32, 33] and that compression work, viscous dissipation, and radiative transport are negligibly small. Thus, the governing equations are given as follows:

conservation of mass

$$\frac{\partial \bar{u}}{\partial \bar{x}}+\frac{\partial \bar{v}}{\partial \bar{y}}=0; \tag{1}$$

Newton's second law

$$\bar{u}\frac{\partial \bar{u}}{\partial \bar{x}}+\bar{v}\frac{\partial \bar{u}}{\partial \bar{y}}=-\frac{1}{\rho_0}\frac{\partial \bar{P}}{\partial \bar{x}}+\nu_0\left(\frac{\partial^2 \bar{u}}{\partial \bar{x}^2}+\frac{\partial^2 \bar{u}}{\partial \bar{y}^2}\right)+g\beta_0(\bar{T}-T_\infty) \tag{2}$$

$$\bar{u}\frac{\partial \bar{v}}{\partial \bar{x}}+\bar{v}\frac{\partial \bar{v}}{\partial \bar{y}}=-\frac{1}{\rho_0}\frac{\partial \bar{P}}{\partial \bar{y}}+\nu_0\left(\frac{\partial^2 \bar{v}}{\partial \bar{x}^2}+\frac{\partial^2 \bar{v}}{\partial \bar{y}^2}\right); \tag{3}$$

conservation of energy

$$(\rho_0 C_{p_0})\left(\bar{u}\frac{\partial \bar{T}}{\partial \bar{x}}+\bar{v}\frac{\partial \bar{T}}{\partial \bar{y}}\right)=K\left(\frac{\partial^2 T}{\partial \bar{x}^2}+\frac{\partial^2 \bar{T}}{\partial \bar{y}^2}\right) \tag{4}$$

where $\bar{u}$ and $\bar{v}$ are the velocity components in the $\bar{x}$- and $\bar{y}$-directions, $\bar{T}$ the temperature, $\bar{P}$ the 'motion pressure' (defined as the actual pressure in fluid less the pressure when the fluid is at rest at uniform temperature, T_0), g the magnitude of the acceleration due to gravity and ρ_0, ν_0, β_0 C_{p_0}, and K_0 are, respectively, the fluid density, kinematic viscosity, coefficient of thermal expansion, constant pressure specific heat, and thermal conductivity of air all evaluated at some reference temperature, T_0.

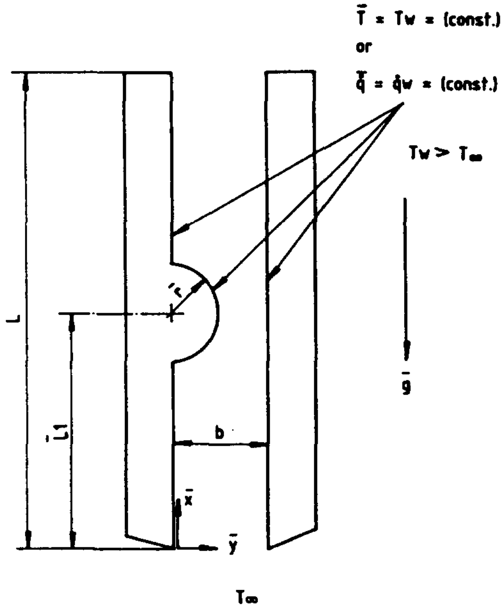

FIG. 1. Geometry of the obstructed channel considered in this investigation.

The boundary conditions for these equations are given by

$$\left.\begin{array}{l}\bar{u}=\bar{v}=0\\ \text{and } \bar{T}=T_w(=\text{const.})\\ \text{or } \dot{q}=q_w(=\text{const.})\end{array}\right\}$$

$$\begin{array}{ll}\text{for } \bar{y}=0 & \text{and } 0\leqslant \bar{x}\leqslant(\bar{L}_1-\bar{r})\\ \text{for } \bar{y}=0 & \text{and } (\bar{L}_1+\bar{r})\leqslant \bar{x}\leqslant L\\ \text{for } \bar{y}=\sqrt{\bar{r}^2-(\bar{L}_1-\bar{x})^2} & \text{and } (\bar{L}_1-\bar{r})\leqslant \bar{x}\leqslant(\bar{L}_1+\bar{r})\end{array} \tag{5}$$

$$\left.\begin{array}{l}\bar{u}=\bar{v}=0\\ \text{and } \bar{T}=T_w(=\text{const.})\\ \text{or } \dot{q}=q_w(=\text{const.})\end{array}\right\} \quad \text{for } \bar{y}=b \quad \text{and} \quad (0\leqslant \bar{x}\leqslant L) \tag{6}$$

$$\left.\begin{array}{l}\bar{v}=0\\ -\bar{P}+\mu\dfrac{\partial \bar{u}}{\partial \bar{x}}=0\\ \partial \bar{T}/\partial \bar{x}=0\end{array}\right\} \quad \text{for } \bar{x}=L \quad \text{and} \quad (0\leqslant \bar{y}\leqslant b) \tag{7}$$

$$\left.\begin{array}{l}\bar{v}=0\\ -\bar{P}+\mu\dfrac{\partial \bar{u}}{\partial \bar{x}}=0\\ \bar{T}=T_\infty\end{array}\right\} \quad \text{for } \bar{x}=0 \quad \text{and} \quad (0\leqslant \bar{y}\leqslant b). \tag{8}$$

In the above boundary conditions, the total stress or traction (τ_{xx}) normal to the boundary at the channel entrance and exit and the heat flux (q_w) normal to the boundary at the channel exit are prescribed equal to zero. These boundary conditions are not required to be explicitly enforced at each node along the entrance or the exit when using the finite element algorithm. Instead they are naturally enforced through the elemental surface integrals generated by the method of weighted residuals (MWR) formulation of the finite element algorithm.

3. NUMERICAL STUDY

The boundary value problem outlined in Section 2 is too complicated for exact solution. Hence, one must resort to the use of a numerical method to obtain a solution for this set of coupled, non-linear, elliptic partial differential equations.

In the present study, the numerical analysis was carried out using a general purpose finite element computer code called NACHOS. The NACHOS computer code is a general purpose computer program designed for the solution of two-dimensional, incompressible fluid dynamic problems. The program capabilities and organization and the derivation of finite element equations on which NACHOS is based have been described in sufficient detail elsewhere [34, 35] and will not be repeated here. However, for the sake of completeness, two essential parts of the NACHOS code (the element library and the solution procedures) will be described.

The elements included in NACHOS consist of isoparametric and subparametric quadrilaterals and triangles. Within each of these elements, the velocity components and temperature are approximated using biquadratic basis functions; pressure is given by a linear approximation. For the analysis of steady-state problems, iterative solution procedures are used. Transient problems are analyzed using a modified Crank–Nicholson procedure.

For the analysis of the obstructed channel outlined in Section 2, a non-uniform mesh of 190 quadrilateral elements was employed. The elements were concentrated near the obstruction and wall boundaries. The computations were made using iterative solution procedures provided in NACHOS. Convergence is defined to have been obtained when the maximum change in temperature is less than 0.5%. As required by NACHOS code, the calculations were actually performed in terms of physical variables.

4. COMPUTATIONAL MATRIX

To set up a computational matrix, equations (1)–(4) outlined in Section 2 are now expressed in terms of the following dimensionless variables and parameters:

$$u = \frac{\bar{u}b^2}{\alpha L};\quad v = \frac{\bar{v}b}{\alpha};\quad x = \frac{\bar{x}}{L};\quad y = \frac{\bar{y}}{b};$$

$$r = \frac{\bar{r}}{L};\quad L_1 = \frac{\bar{L}_1}{L};\quad Pr = \frac{\nu}{a}. \tag{9}$$

For the UWT channel

$$\theta = \frac{(\bar{T}-T_\infty)}{(T_\omega - T_\infty)}$$

and

$$P = \frac{\bar{p}}{g\beta\rho_\infty(T_\omega - T_\infty)L}$$

while for the UHF channel

$$\theta = \frac{(\bar{T}-T_\infty)}{(q_\omega b/k)}$$

and

$$P = \frac{\bar{p}k}{g\beta\rho_\infty q_\omega bL}.$$

The resulting equations are:

conservation of mass

$$\frac{\partial u}{\partial x} + \frac{\partial v}{\partial y} = 0; \tag{10}$$

Newton's second law

$$\frac{1}{Pr}\left[u\frac{\partial u}{\partial x} + v\frac{\partial u}{\partial y}\right] = Ra\left(\frac{b}{L}\right)\left[\theta - \frac{\partial p}{\partial x}\right] + \left[\left(\frac{b}{L}\right)^2\frac{\partial^2 u}{\partial x^2} + \frac{\partial^2 u}{\partial y^2}\right] \tag{11}$$

$$\frac{1}{Pr}\left(\frac{b}{L}\right)^2\left[u\frac{\partial v}{\partial x} + v\frac{\partial v}{\partial y}\right] = -Ra\left(\frac{b}{L}\right)\frac{\partial p}{\partial y} + \left(\frac{b}{L}\right)^2\left[\left(\frac{b}{L}\right)^2\frac{\partial^2 v}{\partial x^2} - \frac{\partial^2 v}{\partial y^2}\right]; \tag{12}$$

energy conservation

$$u\frac{\partial \theta}{\partial x} + v\frac{\partial \theta}{\partial y} = \left(\frac{b}{L}\right)^2\frac{\partial^2 \theta}{\partial x^2} + \frac{\partial^2 \theta}{\partial y^2} \tag{13}$$

where the Rayleigh number, Ra, is given by

$$Ra = Pr\,Gr = Pr\frac{\beta g(T_\omega - T_\infty)b^3}{\nu^2}$$

for the UWT case; or

$$Ra = Pr\frac{\beta g q_\omega b^4}{\nu^2 k}$$

for the UHF case.

The boundary conditions for equations (10)–(13) are

$$\left.\begin{array}{l} u = v = 0 \\ \text{and } \theta = 1 \\ \text{or } \partial\theta/\partial y = -1 \end{array}\right\}$$

for $y = 0$ and $0 \leqslant x \leqslant (L_1 - r)$

for $y = 0$ and $(L_1 + r) \leqslant x \leqslant 1$

for $y = (L/b)\sqrt{(r^2 - (L_1 - x)^2)}$ and $(L_1 - r) \leqslant x \leqslant (L_1 + r)$ (14)

$$\left.\begin{array}{l} u = v = 0 \\ \text{and } \theta = 1 \\ \text{or } \partial\theta/\partial y = -1 \end{array}\right\} \quad y = 1 \text{ and } (0 \leqslant x \leqslant 1) \tag{15}$$

$$\left.\begin{array}{l} v = 0 \\ -P + \left(\dfrac{b}{L}\right)\dfrac{1}{Ra}\dfrac{\partial u}{\partial x} = 0 \\ \partial\theta/\partial x = 0 \end{array}\right\}$$

$$\text{for } x = 1 \text{ and } (0 \leqslant y \leqslant 1) \tag{16}$$

$$\left.\begin{array}{l} v = 0 \\ -P + \left(\dfrac{b}{L}\right)\dfrac{1}{Ra}\dfrac{\partial u}{\partial x} = 0 \\ \theta = 0 \end{array}\right\}$$

$$\text{for } x = 0 \text{ and } (0 \leqslant y \leqslant 1). \tag{17}$$

From equations (10)–(17), the dimensionless parameters of interest in the problem are the Rayleigh number (Ra), the dimensionless distance of the obstruction center line above the bottom of the channel (L_1), and the dimensionless obstruction radius (r). The numerical calculations were performed for 31 different cases. Nine of these cases were run for the unobstructed channel ($r = 0$); of which eight cases were for the constant wall temperature boundary condition and one case for the uniform wall heat flux. The solutions for these cases were obtained for comparison with those of other authors in order to verify the code and the accuracy of the numerical procedure. Twenty-one of the remaining 22 cases were run for the obstructed channel ($r = 0.091$) with the uniform wall temperature boundary condition; one case was run for the obstructed channel with the uniform heat flux boundary condition. The cases for the obstructed channel were performed since it is the primary interest of the present study. The computational matrices are shown in Tables 1 and 2.

Table 1. Computational matrix for cases with uniform wall temperature boundary conditions

Unobstructed channel Ra'	Obstructed channel ($r = 0.091$) Ra	L_1	AR
3.5×10^2	6.8×10	0.50	0.1364
			0.1818
6.4×10^2	1.3×10^2	0.50	0.1364
			0.1818
			0.2727
1.0×10^3	3.4×10^2	0.50	0.1364
			0.1818
			0.2727
2.5×10^3	1.0×10^3	0.50	0.1364
			0.1818
			0.2727
5.5×10^3	2.6×10^3	0.50	0.1364
			0.1818
			0.2727
1.0×10^4	6.0×10^3	0.50	0.1818
			0.2727
1.8×10^4	2.0×10^4	0.50	0.2727
—	5.0×10^4	0.50	0.3636
2.0×10^2	9.0×10^2	0.25	0.2182
—	9.0×10^2	0.50	0.2182
—	9.0×10^2	0.91	0.2182

Table 2. Computational matrix for cases with uniform heat flux boundary conditions

Unobstructed channel	Obstructed channel ($r = 0.091$)		
Ra'	Ra	L_1	AR
5.0×10^2	2.3×10^3	0.50	0.2182

5. EXPERIMENTAL STUDY

The objectives of the experimental investigation were:

(1) To characterize qualitatively (through flow visualization) and quantitatively (through optical measurements) the structure of the natural convection flow field in air in a two-dimensional, isothermal channel with a single obstruction.

(2) To check by direct comparison with experimental measurements the accuracy of the numerical solutions. A detailed description of the experimental apparatus, instrumentation, and flow visualization is given in ref. [31]. The experiments were performed for an obstructed vertical channel of $L_1 = 0.5$, $r = 0.091$, with $\Delta T = 30$ K and values of Ra that ranged from 10^2 to 10^4 (Fig. 1). For each experiment, the following steps were performed.

(a) Interferograms were made with a Wollaston Prism Interferometer (WPI) [36–38]. The local average heat transfer coefficients were determined by reading these interferograms. A reproduction of one is shown in Fig. 2.

(b) A flow visualization test was performed and the results were recorded.

(c) Structural (plate and enclosure wall) temperature and air temperatures in the enclosure and the laboratory were recorded.

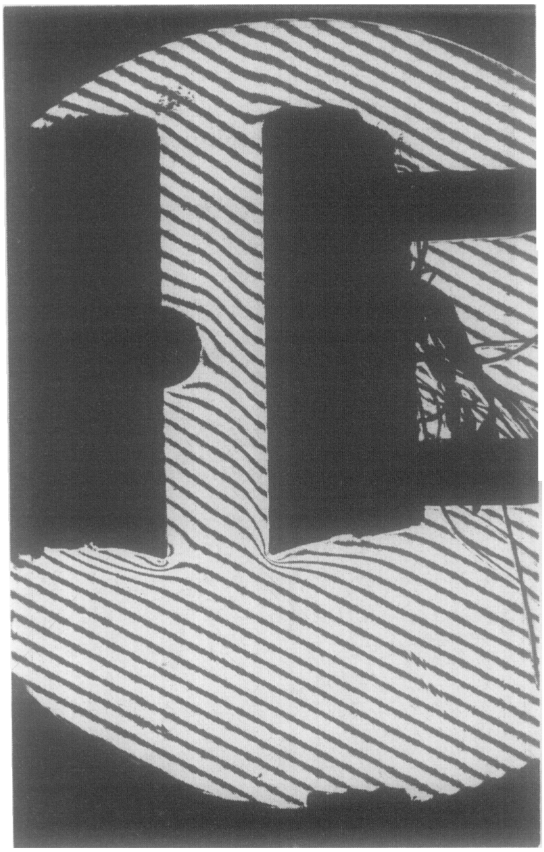

FIG. 2. Wollaston prism interferometer fringe pattern.

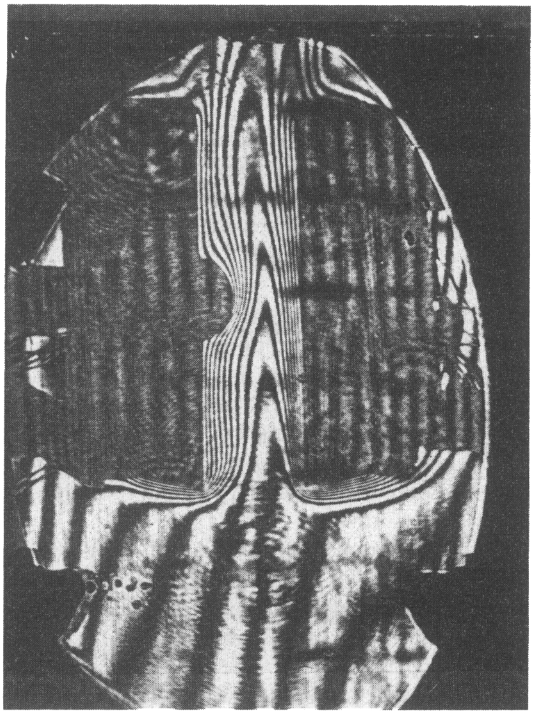

FIG. 3. Mach–Zehnder interferometer infinite fringe pattern.

(d) Mach–Zehnder Interferometer (MZI) interferograms were made [39] in the infinite fringe setting, producing a fringe pattern to represent the isotherms. A reproduction of one of these interferograms is shown in Fig. 3.

(e) A Mach–Zehnder Interferometer (MZI) interferogram was made [39] in the wedge fringe setting. Each interferogram was recorded photographically and a reproduction of one is shown in Fig. 4. The temperature distribution in the channel was determined from the interferogram.

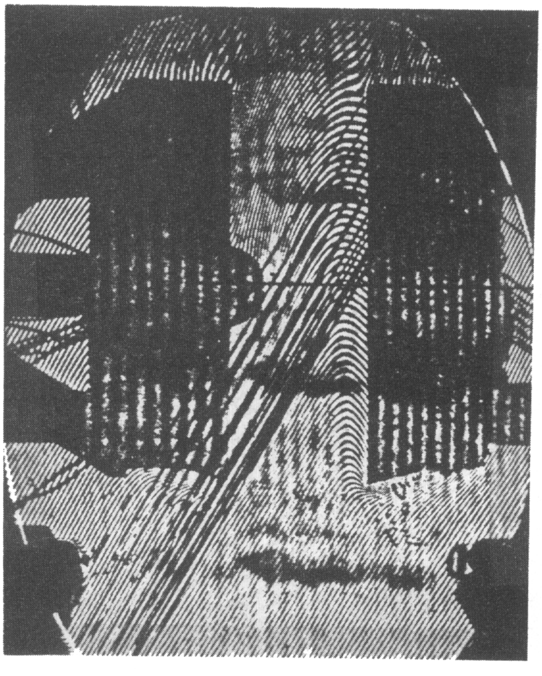

FIG. 4. Mach–Zehnder interferometer wedge fringe pattern.

The estimated uncertainty associated with the experimental values of the heat transfer coefficients (h_{conv}) is approximately 19% [31], while the one associated with the experimental values of temperature is 0.44°C [31].

6. RESULTS AND DISCUSSION

Results were obtained from the numerical solution for air for both uniform wall temperature and uniform wall heat flux conditions for all the cases shown in Tables 1 and 2. Results were also obtained for these cases from the experimental data for air for the uniform wall temperature condition. The solutions for these conditions in the different cases are discussed individually in the following sections (Sections 6.1 and 6.2).

6.1. *Uniform wall temperature*

For the unobstructed channel ($r = 0$) with UWT boundary conditions, typical local heat transfer coefficients and average Nusselt number (Nu) calculations were carried out. In Fig. 5, Nu is plotted against Ra for $Pr = 0.72$, and a comparison is made between the numerical results of this investigation, the numerical work of Bodia and Osterle [5], the experimental work of Elenbass [21], and the present experimental work. The comparison shows excellent agreement (within an average difference of 3%). The experimental results are systematically low.

For the obstructed vertical channel with isothermal walls, solutions were obtained for the local Nusselt numbers (Nu_x). Figure 6 shows a comparison between local Nusselt numbers from the numerical solutions and those obtained from the experimental data using the Wollaston Prism Interferometer. There is close agreement between the theoretical and experimental results, except near the entrance to the channel ($x/L \leqslant 0.1$).

At lower values of the Rayleigh number (Ra), the effect of the obstruction on heat transfer from the unobstructed wall is shown by the curve of local Nusselt numbers (Nu_x) along the wall. As can be seen from Fig. 6, at a point along the wall, the local Nusselt number (Nu_x) increases with distance up the wall, then decreases and then increases again. The same trend can be observed for the obstructed wall curves for all Rayleigh numbers (Ra) [31]. The lowest values of the local Nusselt number (Nu_x) are obtained at the two intersections between the obstruction and the wall. As the velocity of the flow increases in the vicinity of the obstruction, the heat transfer coefficient increases to a maximum value and then decreases further up the channel where the velocity decreases to a minimum value and then increases again.

The average Nusselt numbers (Nu) from the numerical solution as well as those obtained from the

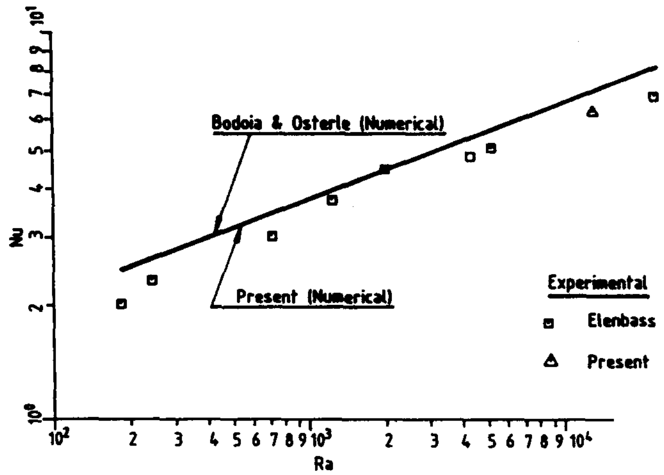

FIG. 5. Comparison between the present solution and those of Bodoia and Osterle [5] and Elenbass [21] for the unobstructed channel.

experimental data are plotted against the Rayleigh number (Ra) (on a log–log plot) for different aspect ratios (AR) in Fig. 7. The numerical results and the measurements are seen to agree within an average deviation of 5% with a maximum deviation of 6.25%. There are no experimental data points at lower Rayleigh numbers (Ra). To obtain lower Rayleigh numbers (Ra), either the temperature difference (ΔT) or the distance between the two vertical plates should be decreased. A small temperature difference will result in very small fringe shifts which will be difficult to measure and because of the obstruction size the distance between the plates can only be decreased to a certain value. Because of these two constraints, experimental data points were not taken at lower Rayleigh numbers (Ra).

From the non-dimensional governing equations and boundary conditions, it can be seen that the non-dimensional parameters are the Rayleigh number (Ra), the aspect ratio (AR), the obstruction size (r),

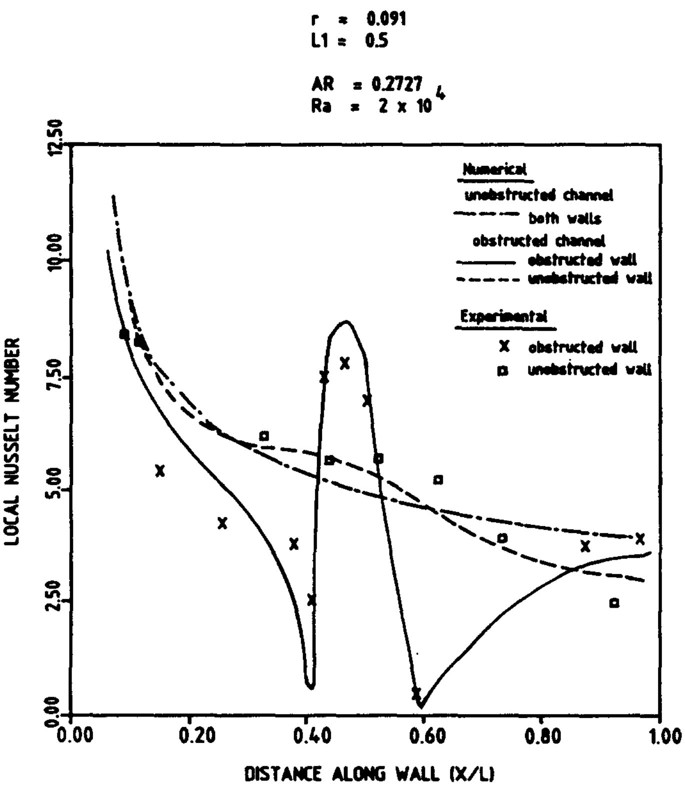

FIG. 6. Comparison of numerical and experimental results for the local Nusselt number (Nu_x).

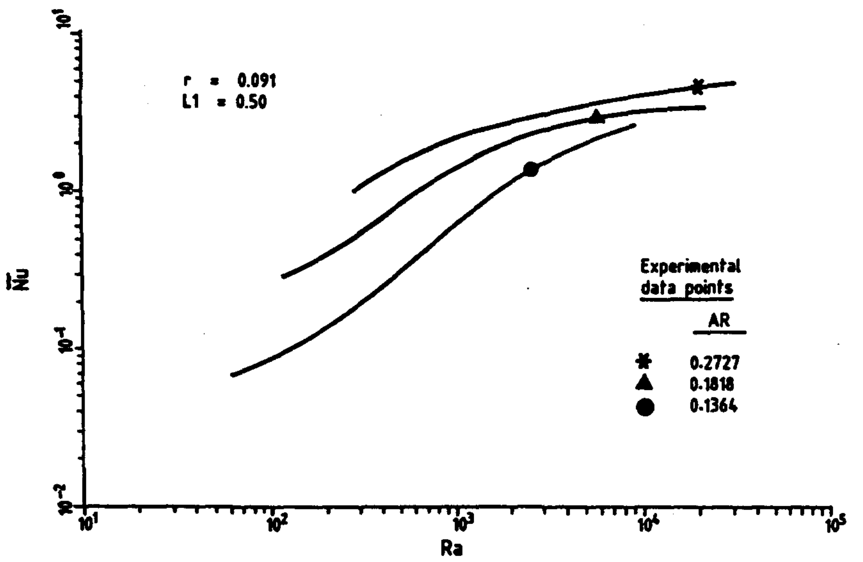

FIG. 7. Comparison of the computed and measured Nusselt numbers for the obstructed channel.

and the obstruction location (L_1). For constant r and L_1, the average Nusselt number (Nu) will be a function of the Rayleigh number (Ra) and the aspect ratio (AR). Figure 7 shows that as the Rayleigh number increases the effect of the aspect ratio (AR) decreases. This can also be observed from the non-dimensional form of the governing equations by noting that the aspect ratio term multiplies the terms which can reasonably be expected to be relatively small, e.g. the term in the energy equation representing conduction in the streamwise (x) direction. As the Rayleigh number (Ra) decreases the effect of the aspect ratio increases. This is to be expected, because for lower Rayleigh numbers the flow approaches a fully developed channel flow.

Since one of the primary objectives of this research is to study the effect of obstruction on natural convection flows in vertical channels, the average numbers (Nu) from the numerical solution for both unobstructed and obstructed channels are plotted in Fig. 8 against the Rayleigh number (Ra'), which is defined as ($Ra\,AR$). The curve for the unobstructed channel shown in Fig. 8 is taken from the study of Churchill and Usagi [3]. This curve represents the three flow regimes (fully developed, transition, and isolated vertical flat plates) for the unobstructed channel, while the one for the particular obstructed channel considered represents only two flow regimes (transition and isolated vertical plates). If the obstructed channel is longer, the fully developed regime should also be present. A comparison of these curves shows that the presence of the obstruction causes a significant

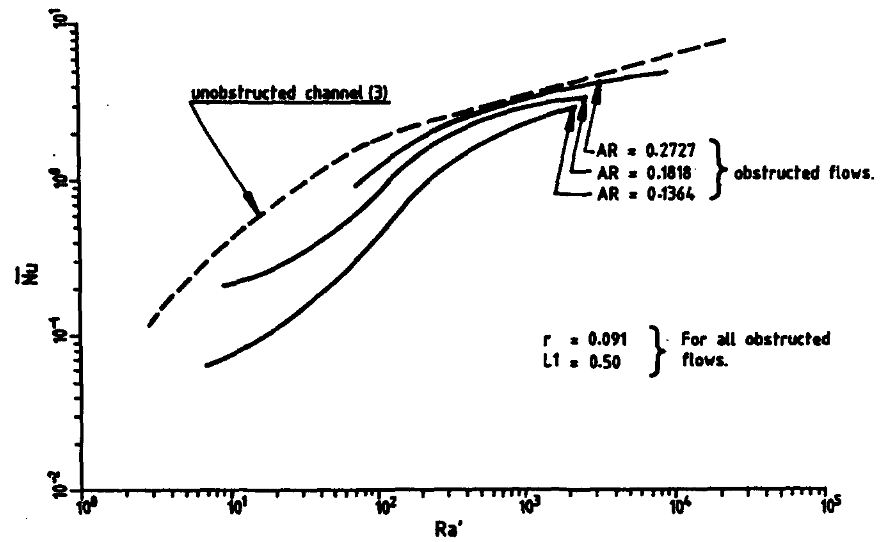

FIG. 8. Comparison of the computed average Nusselt numbers for the obstructed and unobstructed channel flows.

reduction in the Nusselt number in the transition flow regime for the obstructed channel. It ranges from about 5% at a Rayleigh number of 10^4 to 40% at a Rayleigh number of 10. This is caused by the reduction of flow area due to the presence of the obstruction. Although the reduction in the cross-sectional area of the channel increased the velocity of the flow around the tip of the obstruction and thereby increased the local heat transfer rate in that area, this does not compensate for the reduced flow rate due to area reduction. The regions of recirculating flow which are formed above and below the obstruction also affect the heat transfer, since the heat is transferred across the recirculating regions by conduction only. The regions of recirculating flow at the bottom of the obstruction are usually quite small and they are detected in the numerical results by examining the streamline values at those nodes. The experimental observations of these circulating flow regions provide a similar trend to the numerical observations.

The computed streamlines and isotherms for the same case are shown in Fig. 9. From the streamlines, it can be seen that the density of the streamlines increases in the region around the tip of the obstruction, owing to the reduction of the channel's cross-sectional areas. Hence, the flow speeds up in this region. From the isotherm plots [31], it can be seen that in the case of a very large Rayleigh number, a boundary layer is formed on each plate. Figure 3 shows a reproduction of the Mach–Zehnder interferogram and illustrates how fringe lines map out constant temperature lines (isotherms). Physical observations of streamlines through flow visualization and of isotherms through interferograms (in the infinite fringe setting) show a good qualitative agreement with the numerical results.

The computed temperature profiles from the numerical solution at $x/L = 0.5$ and 1 are indicated in Fig. 10. It can be seen from Figs. 43–46 of ref. [31] that as the Rayleigh number increases the minimum temperature at these two planes ($x/L = 0.5$ and 1) decreases and the minimum also shifts to lower values of x/L since the boundary layer thickness decreases as x/L decreases.

The computed velocity profiles from the numerical solution at $x/L = 0, 0.5$ and 1 are indicated in Fig. 11. It can be seen that the entrance velocity profile appears to be parabolic when the entrance velocity distribution is determined by applying the natural boundary condition. The maximum velocity occurs at mid-plane ($x/L = 0.5$) owing to the reduction of the channel's cross-sectional area. As the Rayleigh number increases, the maximum velocity in the channel increases as shown in Figs. 47–50 of ref. [31].

Figure 12 shows a comparison between temperature profiles obtained numerically and experimentally. The measurements and the numerical results are seen to agree within an average deviation of 6% and maximum deviation of 10%.

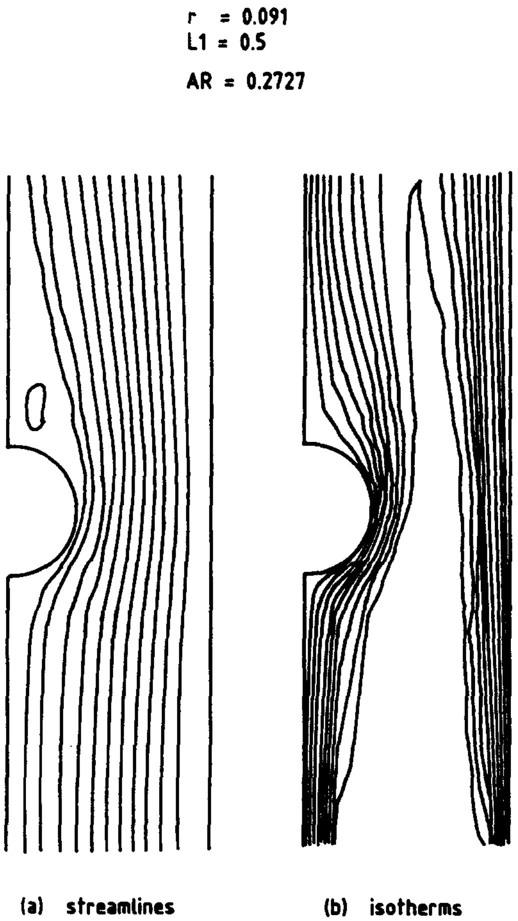

FIG. 9. Computed streamlines and isotherms for $Ra = 2.0 \times 10^4$.

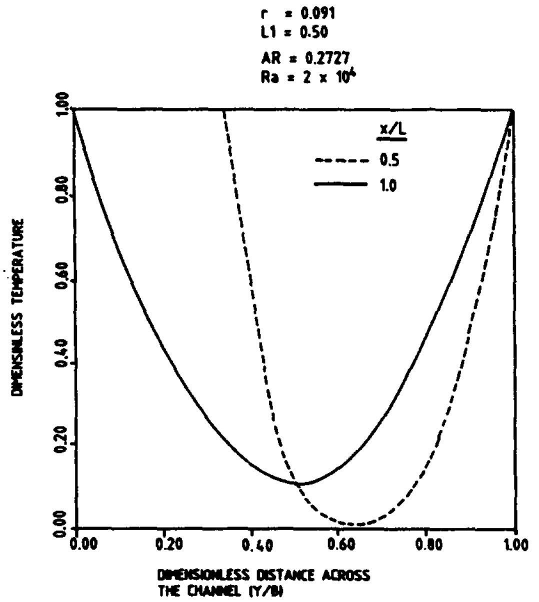

FIG. 10. Transverse temperature distributions in the obstructed channel.

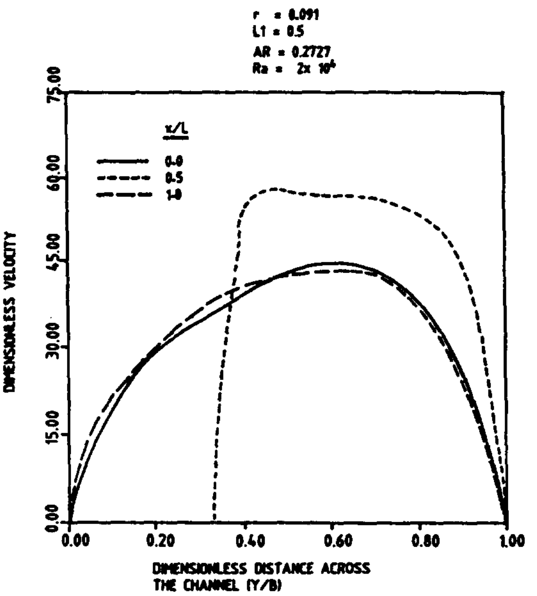

FIG. 11. Transverse velocity distributions in the obstructed channel.

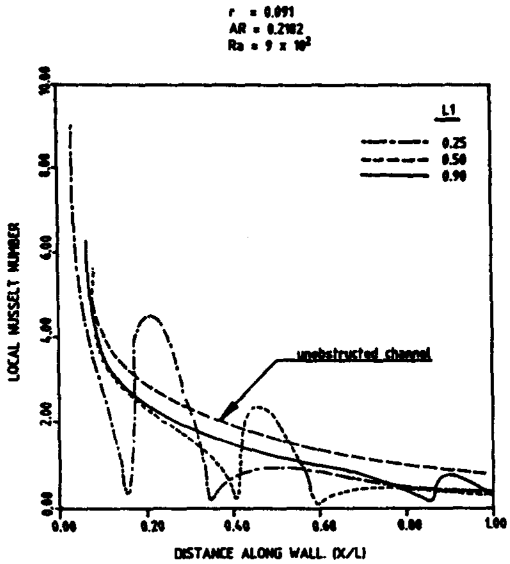

FIG. 13. Variation of local Nusselt number with elevation in channel wall for different values of L_1.

Finally, in summary, the presence of an obstruction in the channel causes the vertical flow to increase near the obstruction and the surface area on the obstructed wall to increase (both should increase the heat transfer rate). However, the average Nusselt number decreased when compared to that for the unobstructed channel. This is due to the reduction of mass flow rate and the existence of the regions of recirculating flow caused by the presence of the obstruction in the channel.

For the obstructed vertical channel with isothermal walls ($r = 0.091$) and $L_1/L = 0.25$, 0.5, and 0.91 the numerical solutions were obtained for the local and average Nusselt numbers and the mass flow rates. These values were compared to examine the effect on heat transfer rates of moving the obstruction along the wall. The comparison is shown graphically in Figs. 52 and 53 of ref. [31]. From these figures [31] it can be seen that, for the obstructed channels, as the value of L_1/L increases (or the obstruction is moved away from the channel entrance), both the average Nusselt number and the mass flow rate decrease. As expected, both of these values are less than those obtained for the unobstructed channel. The question which arises is: "Why should the Nusselt number decrease as L_1/L increases?"

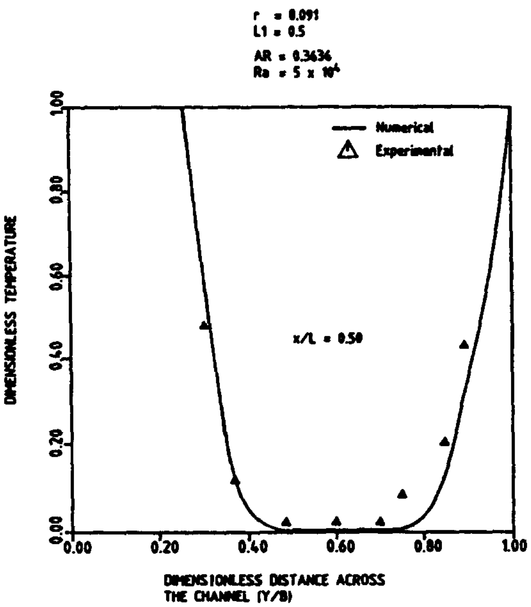

FIG. 12. Comparison between the computed and measured temperature at $x/L = 0.5$ for the obstructed channel.

In an attempt to find a reasonable answer, the local Nusselt number (Nu_x) along the obstructed walls is plotted in Fig. 13, and the isotherms for $L_1/L = 0.25$, 0.5, and 0.91 are shown in Fig. 14. It can be seen from Fig. 13 that the maximum values of the local Nusselt number (Nu_x) near the obstruction decrease as L_1/L increases. From Fig. 14, it can be noted that as L_1/L increases, the temperature at the channel exit plane increases. It can also be noted for this figure that as L_1/L decreases, the boundary layer thickness at the channel entrance decreases and, hence, the temperature gradient at the wall increases as L_1/L decreases. Therefore, the Nusselt number, which is a function of temperature gradient, increases as L_1/L decreases.

6.2. *Uniform wall heat flux*

For the vertical channel with uniform heat flux, solutions are obtained for heat flux values of 13 W m^{-2}. Computed temperature distributions along the walls are shown in Fig. 15. The maximum temperature

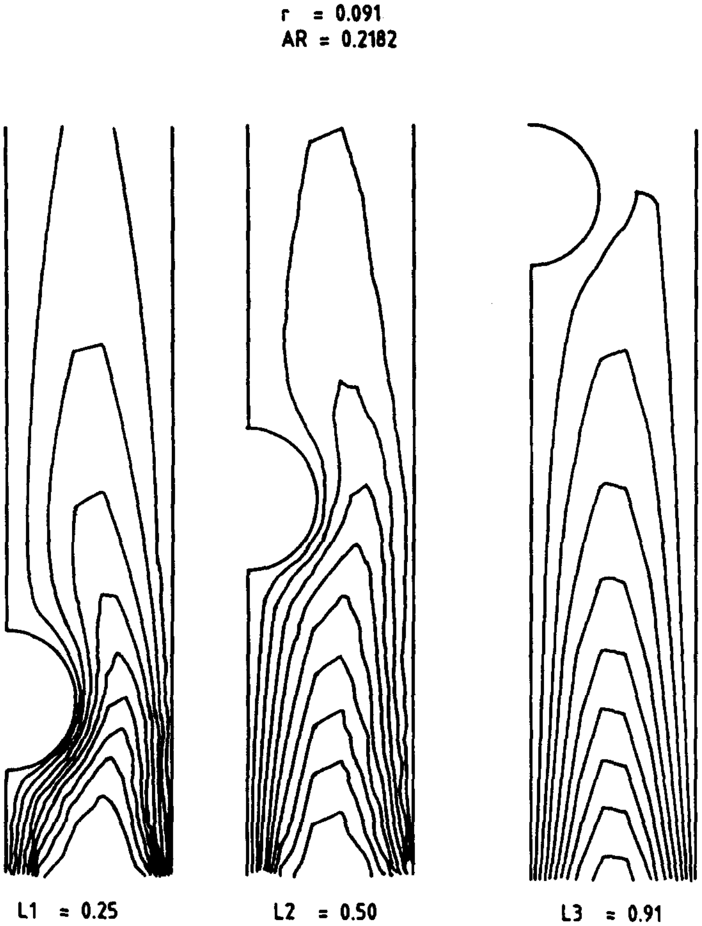

FIG. 14. Computed isotherms for $Ra = 9 \times 10^2$ and different values of L_1.

along the two walls of the obstructed channel occurs at the corner at the top of the obstruction. This is expected because of the region of recirculating flow at that location. The maximum wall temperature in the obstructed channel is, however, only about 4% greater than the maximum temperature in the unobstructed channel. This is not a significant difference.

7. CONCLUSIONS

Natural convective heat transfer in parallel plate vertical channels in air, with and without an internal obstruction, has been studied numerically and experimentally for a Prandtl number of 0.72 and over a range of Rayleigh number from 10^2 to 10^4. Two thermal conditions of the parallel walls are considered: uniform wall temperature (UWT) and uniform heat flux (UHF). A comparison of the average Nusselt number with those reported by other authors shows close agreement.

The results for the obstructed channel with the UWT boundary condition and $L_1 = 0.5$ showed that as the Rayleigh number increases, the Nusselt

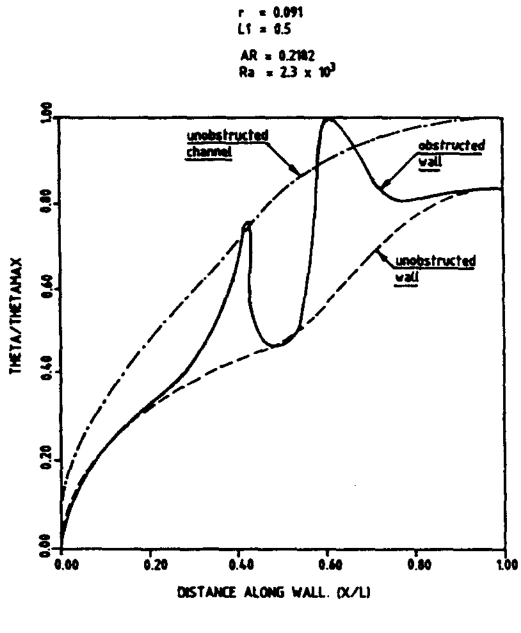

FIG. 15. Axial variations of the wall tempertures of UHF.

number, the quantity of flow, and the maximum velocity increase. However, with increasing Rayleigh number the minimum temperature at the exit decreases. The comparison between the measurements and the numerical results shows close agreement. From the plot of the average Nusselt number versus Rayleigh number for different aspect ratios (Fig. 8), it is noted that for $Ra > 10^3$ the effect of the aspect ratio is small, while for $Ra < 10^3$ it is significant.

Comparison of the average Nusselt numbers for the obstructed channel with those for the unobstructed channel shows a reduction in heat transfer for the obstructed channel which ranges from 5% at a Rayleigh number of 10^4 to 40% at a Rayleigh number of 10.

It is found that moving the obstruction along the wall from the leading edge to the exit causes a reduction in the heat transfer rate in the channel. Moving the obstruction from the location $L_1/L = 0.25$ to $L_1/L = 0.5$ resulted in a reduction of about 16% in the magnitude of the average Nusselt number.

For the vertical channel whose walls are heated uniformly, the presence of the obstruction increased the magnitude of the maximum temperature by 4%. The maximum temperature occurred at the corner at the top of the obstruction and not at the exit as is the case for unobstructed channels.

Finally, virtually nothing was previously known about the detailed nature of obstructed natural convection flows in channels. Based on the present investigation, however, we can conclude that the presence of an obstruction and its location have significant effects on natural convection flows in vertical channels. This is an open-ended research area. Hopefully, the present study will serve to whet the appetite of other investigators to become involved in this area of research. The effect of different obstruction geometries and locations with different thermal boundary conditions needs to be investigated both experimentally and numerically. Multiple obstruction and obstruction on both walls also need investigation.

Acknowledgement—The first author would like to thank King Fahd University of Petroleum and Minerals for its support during his study at UTK.

REFERENCES

1. W. Aung and B. Chimah, Laminar heat exchange in vertical channels—applications to cooling of electronic systems. In *Low Reynolds Number Flow Heat Exchange* (Edited by S. Kakac, R. K. Shah and A. E. Bergles), p. 395. Hemisphere, Washington, DC (1983).
2. Y. Jaluria, Natural convection cooling of electronic equipment. In *Natural Convection, Fundamentals and Applications*, p. 961. Hemisphere, Washington, DC (1985).
3. A. D. Kraus and A. Bar-Cohen, *Thermal Analysis and Control of Electronic Equipment*. McGraw-Hill, New York (1983).
4. R. K. Engel and W. K. Mueller, An analytical investigation of natural convection in vertical channels. ASME Paper No. 67-HT-16. Presented at the ASM–AIChE Heat Transfer Conf., Seattle, Washington, 6–8 August (1967).
5. J. R. Bodoia and J. F. Osterle, The development of free convection between heated vertical plates, *ASME J. Heat Transfer* **84**, 40–44 (1962).
6. W. Aung, L. S. Fletcher and V. Sernas, Development of laminar free convection between vertical flat plates with asymmetric heating, *Int. J. Heat Mass Transfer* **15**, 2293–2328 (1972).
7. O. Miyatake, M. Fujii and T. Tanaka, Natural convection heat transfer between vertical parallel plates—one plate with a uniform heat flux and the other thermally insulated, *Heat Transfer—Jap. Res.* **4**, 25–33 (1973).
8. O. Miyatake and T. Fujii, Free convectic heat transfer between vertical parallel plates—one plate isothermally heated and the other thermally insulated, *Heat Transfer—Jap. Res.* **3**, 30–38 (1972).
9. W. Aung, K. E. Beitin and J. J. Kessler, Natural convection cooling of electronic cabinets containing arrays of vertical circuit cards, ASME Paper No. 72-WA/HT-40. Presented at the ASME Winter Annual Meeting, New York, 26–30 November (1972).
10. J. C. Coyne, An analysis of circuit board temperatures in electronic equipment frames cooled by natural convection. In *Fundamentals of Natural Convection/Electronic Equipment Cooling* (Edited by L. C. Witte and L. S. Saxena), ASME Publication No. HTD-Vol. 32, pp. 59–65 (1984).
11. C. F. Kettleborough, Transient laminar free convection between heated vertical plates including entrance effects, *Int. J. Heat Mass Transfer* **15**, 883–896 (1972).
12. H. Nakamura, Y. Asako and T. Naiton, Heat transfer by free convection between two parallel flat plates, *Numer. Heat Transfer* **5**, 95–106 (1982).
13. T. Burch, T. Rhodes and S. Acharya, Laminar natural convection between finitely conducting vertical plates, *Int. J. Heat Mass Transfer* **28**, 1173–1186 (1985).
14. J. R. Carpenter, D. G. Briggs and V. Sernas, Combined radiation and developing laminar free convection between vertical flat plates with asymmetric heating, *J. Heat Transfer* 95–98 (February 1976).
15. T. Aihara, Effects of inlet boundary-conditions on numerical solutions of free convection between vertical parallel plates, *Rep. Inst. High Speed Mech.* **28**, 1–27 (1973).
16. K. C. Karki and S. V. Patankar, Cooling of a vertical shrouded fin array by natural convection: a numerical study. In *Fundamentals of Natural Convection/Electronic Equipment Cooling* (Edited by L. C. Witte and L. S. Saxena), ASME Publication No. HTD-Vol. 32, pp. 33–40 (1984).
17. Ramakrishna, Rubin and Khosla, Laminar natural convection along vertical square ducts, *Numer. Heat Transfer* **5**, 59–79 (1982).
18. L. P. Davis and J. J. Perona, Development of free convection flow in a heated vertical open tube, *Int. J. Heat Mass Transfer* **14**, 889–903 (1971).
19. R. Kageyama and M. Izumi, Natural heat convection in a vertical circular tube, *Bull. ASME* **13**, 382–394 (1970).
20. J. R. Dyer, The development of natural convection flow in a vertical uniform heat flux duct, *Int. J. Heat Mass Transfer* **18**, 1455–1465 (1965).
21. W. Elenbass, Heat dissipation of parallel plates by free convection, *Physica* **9**, 1–28 (1942).
22. V. Sernas, L. Fletcher and W. Aung, Heat transfer measurements with a Wollaston Prism Schileren Interferometer, ASME Paper No. 72-HT-9. Presented at the AIChE–ASME Heat Transfer Conf., Denver, Colorado, 6–9 August (1972).
23. E. M. Sparrow and P. A. Bahrami, Experiments in natural convection from vertical parallel plates with either open or closed edges, *ASME J. Heat Transfer* **102**, 221–227 (1980).
24. H. T. Akbari and R. Borges, Finite convective laminary flow within Trombe wall channel, *Solar Energy* **22**, 165–174 (1979).

25. J. A. Tichy, The effect of inlet and exit losses on free convective laminary flow in the Trombe wall channel, ASME Paper No. 82-WA/Sol-10 (1982).
26. E. K. Levy, P. A. Eichen, W. R. Cintani and R. R. Shaw, Optimum plate spacings for laminar natural convection heat transfer from parallel vertical isothermal flat plates: experimental verification, *ASME J. Heat Transfer* **97**, 474–476 (1975).
27. S. W. Churchill, A comprehensive correlating equation for buoyancy-induced flow in channels, *Lett. Heat Mass Transfer* **4**, 193–199 (1977).
28. E. M. Sparrow and C. Prakash, Enhancement of natural convection heat transfer by a staggered array of discrete vertical plates, *ASME J. Heat Transfer* **102**, 215–220 (1980).
29. C. Prakash and E. M. Sparrow, Performance evaluation for discrete (in-line or staggered) and continuous-plate arrays, *Numer. Heat Transfer* **3**, 89–106 (1980).
30. W. Aung and Y. Yener, Research directions in natural convection. In *Natural Convection—Fundamentals and Applications* (Edited by S. Kakac, W. Aung and R. Viskanta). Hemisphere, Washington, DC (1985).
31. S. A. M. Said, An analytical and experimental investigation of natural convection heat transfer in vertical channels with a single obstruction, Ph.D. Dissertation, University of Tennessee, Knoxville (1986).
32. Y. Jaluria, *Natural Convection Heat and Mass Transfer*. Pergamon Press, New York (1980).
33. P. C. T. deBoer, Thermally driven motion of strongly heated fluids, *Int. J. Heat Mass Transfer* **27**, 2239–2251 (1984).
34. D. K. Gartling, NACHOS—A finite element computer program for incompressible flow problems, Part I—theoretical background, SAND 77-1333, Sandia Laboratories, Albuquerque, New Mexico (1978).
35. D. K. Gartling, NACHOS—A finite element computer program for incompressible flow problems, Part II—user's manual, SAND 77-77-1333, Sandia Laboratories, Albuquerque, New Mexico (1978).
36. Y. Heidari and J. R. Parsons, The UTK Dept. of Mechanical Engineering and Aerospace Engineering, Wollaston Prism Interferometer, Rep. No. MAE NCL-2, University of Tennessee, Knoxville (1985).
37. R. J. Irby and J. R. Parsons, Examination of natural convection from selected downward-facing heated surfaces with the Wollaston Prism Interferometer, Technical Rep. No. MAE NCL-3, University of Tennessee, Knoxville (1985).
38. V. Sernas, The Wollaston Prism Interferometer, Von Karman Institute for Fluid Dynamics Lecture Series 6, *Adv. Measurement Tech. Fluid Mech.*, 7–11 March (1977).
39. J. W. Jessee, The development of a natural convection program for incompressible flow problems, Part II—user's manual, SAND 77-1334, Sandia Laboratories, Albuquerque, New Mexico (1978).

RECHERCHE ANALYTIQUE ET EXPERIMENTALE SUR LA CONVECTION THERMIQUE NATURELLE DANS DES CANAUX VERTICAUX AVEC UNE OBSTRUCTION UNIQUE

Résumé—On étudie expérimentalement et numériquement la convection thermique naturelle laminaire de l'air dans un canal vertical ayant une seule obstruction. Dans l'étude expérimentale, on utilise les techniques optiques pour obtenir à la fois des données quantitatives (flux thermiques et températures) et qualitatives (visualisation de l'écoulement). On ne considère que des conditions de température pariétales uniformes (UWT) dans les expériences. Dans les calculs, on utilise un code général aux éléments finis appelé NACHOS et on considère des conditions aux limites de température pariétale uniforme (UWT) et de flux uniforme (UHF). Les résultats expérimentaux et numériques sont en bon accord. Ils montrent que pour les conditions UWT, la présence d'une obstruction réduit de 5% le nombre de Nusselt moyen à un nombre le Rayleigh de 10^4 et de 40% environ lorsque le nombre de Rayleigh est égal à 10. Quand l'obstruction est déplacée depuis l'entrée jusqu'à la sortie, le coefficient moyen de convection diminue. Pour les conditions UHF, la température maximale (à l'intersection du bord supérieur de la cloison et de la paroi) est seulement de 4% plus grande que la température maximale pour un canal sans obstruction (elle apparait à la sortie du canal).

ANALYTISCHE UND EXPERIMENTELLE UNTERSUCHUNG DES WÄRMEÜBERGANGS BEI NATÜRLICHER KONVEKTION IN SENKRECHTEN KANÄLEN MIT EINEM HINDERNIS

Zusammenfassung—Die laminare natürliche Konvektionsströmung von Luft in einem senkrechten Kanal mit einem einzelnen Hindernis wurde experimentell und numerisch untersucht. In den Experimenten wurden optische Verfahren angewandt zur Ermittlung quantitativer (Wärmeströme und Temperaturen) und qualitativer Ergebnisse (Sichtbarmachung der Strömung). Bei den Versuchen wurde mit konstanter Wandtemperatur gearbeitet. Für die numerische Untersuchung wurde ein allgemein anwendbares Finite-Elemente-Programm mit Namen NACHOS verwendet. Numerisch wurden beide Randbedingungen, konstante Wandtemperatur und konstanter Wärmestrom, untersucht. Die experimentellen Ergebnisse stimmen gut überein. Sie zeigen, daß bei aufgeprägter Wandtemperatur ein Hindernis die mittlere Nusselt-Zahl um 5% (für die Rayleigh-Zahl 10^4) bzw. um 40% (für die Rayleigh-Zahl 10) verringert. Auch die Lage des Hindernisses in Strömungsrichtung beeinflußt den Wärmeübergang. Er nimmt ab, wenn das Hindernis in Richtung Kanalaustritt verschoben wird. Bei aufgeprägtem Wärmestrom ist die maximale Temperatur mit Hindernis nur um 4% höher als ohne Hindernis. Ohne Hindernis tritt sie am Kanalausgang auf, mit Hindernis am Schnittpunkt von Hindernis und Wand.

АНАЛИТИЧЕСКОЕ И ЭКСПЕРИМЕНТАЛЬНОЕ ИССЛЕДОВАНИЕ ЕСТЕСТВЕННОКОНВЕКТИВНОГО ТЕПЛОПЕРЕНОСА В ВЕРТИКАЛЬНЫХ КАНАЛАХ С ОДИНОЧНЫМ ПРЕПЯТСТВИЕМ

Аннотация—Проведено экспериментальное и численое исследование ламинарной естественной конвекции воздуха в вертикальном канале с одночным препятствием. В ходе экспериментального исследования с помощью оптических методов была получена как количественная (тепловые потоки и температурные поля), так и качественная (визуальная картина течения) информация. Эксперименты выплнялись только для постоянных температурных граничных условий на стенках. Для численного исследования использовалась универсальная программа NACHOS. При численных расчетах рассматривались два тепловых граничных условий: постоянная температура и постоянный тепловой поток на стенках. Получено хорошее согласие экспериментальных и численных результатов. Они показывают, что в случае постоянной температуры на стенках наличие препятствия приводит к уменьшению среднего значения числа Нуссельта на 5% при значении числа Рэлея 10^4 и на 40% при значении числа Рэлея 10. Замечено также, что расположение препятствия вдоль стенки приводит к изменению интенсивности теплопереноса. Перемещение препятствия от входа к выходу вызывает уменьшение средней интенсивности теплопереноса для канала. В случае постоянного теплового потока на стенках максимальная температура (которая достигается на пересечении верхнего края препятствия и стенки) лишь на 4% больше максимальной температуры в канале без препятствия (в котором она достигается на выходе).